


LETTER TO THE EDITOR

# On the limitations of using metric radio bursts as diagnostic tools for interplanetary coronal mass ejections

J. Kandekar<sup>1</sup> and A. Kumari<sup>2,\*</sup> 

<sup>1</sup> Department of Physics, Ahmednagar College, Station Road, Ahilyanagar 414001, Maharashtra, India

<sup>2</sup> Udaipur Solar Observatory, Physical Research Laboratory, Dewali, Badi Road, Udaipur 313 001, Rajasthan, India

Received 13 January 2025 / Accepted 15 April 2025

## ABSTRACT

**Aims.** Metric radio bursts are often said to be valuable diagnostic tools for studying the near-sun kinematics and energetics of the interplanetary coronal mass ejections (ICMEs). Radio observations also serve as indirect tools to estimate the coronal magnetic fields. However, how these estimated coronal magnetic fields are related to the magnetic field strength in the ICME at 1 AU has rarely been explored. Our aim was to establish a relation between the coronal magnetic fields obtained from the radio observations very close to the Sun and the magnetic field measured at 1 AU when the ICME arrives at the Earth.

**Methods.** We performed statistical analyses of all metric type II radio bursts in solar cycles 23 and 24 that were found to be associated with ICMEs. We estimated the coronal magnetic field associated with the corresponding CME near the Sun (middle corona) using a split-band radio technique and compared them with the magnetic fields recorded at 1 AU with in situ observations.

**Results.** We found that the estimated magnetic fields near the Sun using radio techniques are not well correlated with the magnetic fields measured at 1 AU using in situ observations. This could be due to the complex evolution of the magnetic field as it propagates through the heliosphere.

**Conclusions.** Our results suggest that while metric radio observations can serve as effective proxies for estimating magnetic fields near the Sun, they may not be as effective close to the Earth. At least, no linear relation could be established using metric radio emissions to estimate the magnetic fields at 1 AU with acceptable error margins.

**Key words.** Sun: activity – Sun: corona – Sun: coronal mass ejections (CMEs) – Sun: heliosphere – Sun: magnetic fields – Sun: radio radiation

## 1. Introduction

The coronal magnetic field ( $B$ ) serves as a fundamental factor governing the formation, evolution, and dynamics of solar corona structures (Dulk & McLean 1978). Measuring these fields directly from observations, particularly in the chromosphere and corona, remains a significant challenge in solar physics (White 2002; Carley et al. 2020, and the references therein). Various methods exist to infer coronal magnetic fields, encompassing techniques such as coronal seismology (Jess et al. 2016), Zeeman splitting of spectral lines (Lin et al. 2004), and extrapolation methods (Wiegmann et al. 2017), though constrained to specific regions of the solar atmosphere. Among these, including the shock-standoff technique (Gopalswamy & Yashiro 2011) and radio techniques, estimations from solar radio bursts offer valuable insights into the coronal magnetic field, especially in the middle corona (Carley et al. 2017).

Solar eruptive phenomena, such as solar flares and coronal mass ejections (CMEs), significantly influence space weather dynamics. These events often trigger energetic electron acceleration, generating radio emissions like type II and type IV bursts observed in the metric and decameter-hectometric (DH) frequency range (Dulk & Suzuki 1980). Taking advantage of

these radio bursts enables the study of the CME early evolution and dynamics near the Sun (within 10 solar radii), which can help in estimating CME magnetic fields and in assessing their geo-effectiveness. Since radio observations consist of solar, heliospheric, and ionospheric space weather phenomena, radio techniques can offer a practical approach to probing the solar atmosphere's magnetic field (White 2004; Gopalswamy 2006). Combining diverse radio techniques with broadband spectroscopic solar radio imaging allows coronal magnetic fields to be derived in various solar regions (Ramesh & Sastry 2000; Kumari et al. 2017a). However, while metric type II radio bursts and their spectral characteristics, such as split-band features, have long served as robust tools for direct coronal magnetic field estimation (Smerd & Sheridan 1974; Vrřnak & Cliver 2008; Mahrous et al. 2018), their correlation with magnetic fields observed at 1 AU during near-Earth interplanetary coronal mass ejections (ICMEs) remains less explored.

Previously, researchers have investigated metric and DH radio bursts and their correlation with electron accelerations, coronal mass ejections (CMEs), and their variations throughout the solar cycle (Kahler et al. 2019; Kumari et al. 2023). However, to the best of our knowledge, no prior study has explored how the characteristics of metric radio bursts can provide insights into space weather phenomena, such as ICMEs. For this study we investigated the long-term datasets of solar radio bursts and ICMEs over solar cycles 23 and 24 to explore the

\* Corresponding author: [anshu@prl.res.in](mailto:anshu@prl.res.in)

feasibility of using radio techniques for coronal magnetic field estimation and their relationship with in situ magnetic field observations at 1 AU during ICME events.

This article is structured as follows. Section 2 discusses the observational data utilized in this study along with detailed data analysis procedures. The findings of the present study are presented in Section 3. Section 4 contains a discussion of the results and their implications, followed by a summary of the study.

## 2. Observations and data analysis

For this study, we identified 88 metric type IIs associated with the ICMEs of solar cycles 23 and 24 (1997–2019). The CME event list used here was obtained from the Coordinated Data Analysis Workshop (CDAW; Yashiro et al. 2004) database<sup>1</sup>, which is a manual catalogue of the CMEs and their properties recorded by the Solar and Heliospheric Observatory's (SOHO) Large Angle and Spectrometric Coronagraph (LASCO) white-light coronagraph observations (Brueckner et al. 1995). This list has the CME properties and parameters such as linear and second-order speed, kinetic energy, mass, angle of position. Additionally, we used the ICME list<sup>2</sup> provided by Richardson & Cane (2010), which contains the dates and times of plasma disturbances of the ICMEs, duration, magnetic field strength, and speed, among other details, and associated with the date and time of the CMEs when they reach 1 AU. This list consists of ICME events since January 1996. Following the CME events associated with the ICME events, the radio data obtained from the Solar Electro-Optical Network (SEON) database<sup>3</sup> was used for the data analysis. It consists of two networks: (1) the Solar Observing Optical Network (SOON) and (2) the Radio Spectral Telescope Network (RSTN). The RSTN contains four solar radio observatories across the globe. The radio database from the Radio Spectral Telescope Network (RSTN) was utilized; this data consists of the Solar Radio Spectrographs (SRS) over a wide band (25–180 MHz), where the Radio Interference Measuring Set (RIMS) is the instrument detecting radio emissions at eight different frequencies. For the missing type IIs in the SEON RSTN database, eCallisto data<sup>4</sup> was referred. Furthermore, Hiraiso Radio Spectrograph (HiRAS) data (Kondo et al. 1995) managed by the National Institute of Information and Communications Technology (NICT<sup>5</sup>) was also utilized to obtain the spectra of type II bursts. We used the OMNI 5 min data from NASA/GSFC's OMNIweb for the related ICMEs. The data was accessed through NASA's Coordinated Data Analysis Web (CDAWeb<sup>6</sup>). We utilized the 5 min high-resolution flow speed (km/s) and the magnetic field (nT) data.

Out of the 88 events identified, only 31 metric type IIs for solar cycles 23 (1996–2008) and 24 (2008–2019) had split-band features identified in the solar dynamic spectra. Few of the type IIs had a start frequency > 180 MHz (Appendix A.1). The 31 CME-ICME associated split-band events comprised a fundamental band and a harmonic band. As shown in Figure 1, these events also exhibited a clear three-part structure (core, cavity and leading edge, Riley et al. 2008). For radio data analysis, the

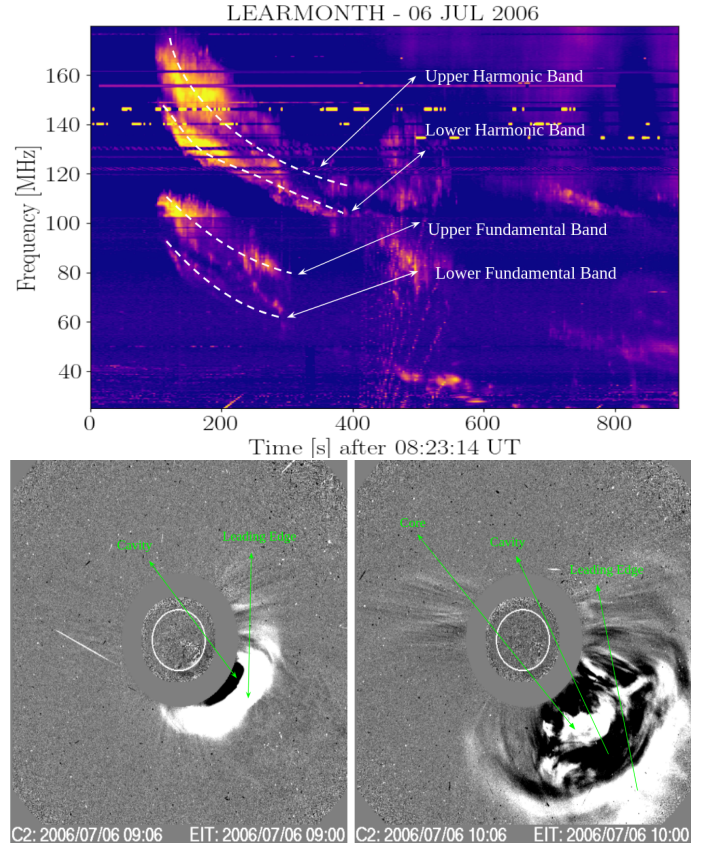


**Fig. 1.** Upper panel: Dynamic spectrum of type II burst recorded by Learmonth Observatory on 6 July 2006 in the range 180–25 MHz. The type II burst started at 08:24 UTC and lasted for 17 minutes. The white dotted lines represent the fundamental and harmonic bands. Lower panel: Three-part structure of the CME with a core, cavity, and leading edge recorded by LASCO C2 on 6 July 2006 at 09:06 UTC and 10:06 UTC. The CME started at 08:54 UTC (Appendix A.1).

dynamic spectra were cleaned and the radio frequency interference was removed. We used the four-fold Newkirk density model (Newkirk 1961) to convert the type II frequencies into radio heights. We used the following equation to estimate the magnetic field strength of 31 split-bands (CME-ICME associated events) (Smerd & Sheridan 1974; Vršnak et al. 2002)

$$B = 5.1 \times 10^{-5} \times F_{LB} \times v_A, \text{ [G]} \quad (1)$$

where  $B$  is the magnetic field strength derived from the type II bursts in gauss,  $F_{LB}$  (MHz) is the lower band frequency of the undisturbed corona (Vršnak et al. 2002), and  $v_A$  (km/s) is the Alfvén speed. The magnetic fields obtained were compared with the magnetic fields recorded at 1 AU. A master list of solar cycle 23 and 24 events was created and divided into two tables. Table A.1 is for type IIs and CME events, and lists date, start time (UT), end time (UT), duration (min), start and end frequency (MHz), start time of CME (UT), CME's width (deg), and CME speed (km/s) obtained from the CDAW database. Table A.2 is for ICME events, and lists date, start time (UT), start and end time of the disturbances in plasma along with its start-end date, ICME Plasma speed (km/s), magnetic field strength (G) obtained from the Richardson–Cane catalogue and the shock speed and the  $B$  field strength (G), which obtained from the radio data analysis of type II burst as described in this section.

<sup>1</sup> <https://cdaw.gsfc.nasa.gov/>

<sup>2</sup> <https://izw1.caltech.edu/ACE/ASC/DATA/level3/icmetable2.htm>

<sup>3</sup> <https://www.ncei.noaa.gov/products/space-weather/legacy-data/solar-electro-optical-network>

<sup>4</sup> <https://www.e-callisto.org/links.html>

<sup>5</sup> <https://solarobs.nict.go.jp/>

<sup>6</sup> <https://cdaweb.gsfc.nasa.gov/>

### 3. Results

#### 3.1. Case study

The dynamic spectra of the slowly drifting type II burst with a fundamental and harmonic band, which occurred on 6 July 2006 at 08:23:12 UT, is displayed in Fig. 1. The CME with a distinct three-part structure begins at 08:54 UT in the lower panel and is subsequently displayed, followed by a disturbance recorded near Earth at 21:36 UT on 9 July 2006 (Richardson & Cane 2010) (Appendix A.2), where the ICME started on 10 July 2006 at 21:00 UT and ended on 11 July 2006 at 19:00 UT, lasting for 22 hours (see Fig. 2). The CME propagated at a speed of 911 km/s, which was higher than the shock speed estimated from the type II radio burst ( $\approx 369$  km/s). The associated speed from the Richardson catalogue was 380 km/s. The difference in speeds of type II, CME, and ICME arises because the CME's interaction with the surroundings affects their speed (Gopalswamy et al. 2000); in this case, we have a CME with a speed of  $\approx 1100$  km/s (Kumari et al. 2023). The split-band type II bursts are seen as well-accepted techniques to estimate magnetic field strengths just above the shock (i.e.  $B$  in gauss derived from the type II radio bursts) (Smerd et al. 1975; Vršnak et al. 2002; Cho et al. 2007; Kumari et al. 2017b). Based on this and as described in Sect. 2, we obtained three values for electron density ( $\text{cm}^{-3}$ ), three values for each  $F_{\text{LB}}$  (MHz) and  $F_{\text{UB}}$  (MHz), three values for heliocentric distance ( $R_{\odot}$ ) for each corresponding value (i.e. six values of heliocentric distance,  $R_{\odot}$ ), and estimated three values of the magnetic field strength ( $B$  (G)). These values served as a basis for our power-law fit equation (Kumari et al. 2019)

$$B = 2 \times r^{-a} \text{ [G]}, \quad (2)$$

where  $B$  is the average magnetic field and  $r$  is the heliocentric distance (in terms of  $R_{\odot}$ , which is the radius of the photospheric Sun). At the range of  $1.36\text{--}1.5 R_{\odot}$  and the lower band frequency range of  $F_{\text{LB}} \approx 141\text{--}101$  MHz, we estimated the average  $B$  field strength of 0.45 G using the Equation (2), for the type II burst that occurred on 6 July 2006. The mean  $B$  (G) field associated with the upstream field just before the ICME ( $B_{1\text{AU}}$  (G)) was found to be  $4.5 \times 10^{-5}$  (G). This associated ICME lasted 22 hours (10 July 2006 21:00 UT to 11 July 2006 19:00 UT). The  $B_{1\text{AU}}$  (G) was significantly attenuated compared to the estimated coronal  $B$  field strength (G), as expected due to the propagation of the CME in the heliosphere and its interaction with other magnetic structures there. Since the magnetic field derived from radio observations were from the lower frequency bands, which can be associated with the undisturbed corona, and the ICME field is, by definition, the disturbed field, we used the  $B$  fields from the upstream field (pre-shock region). For this study we also explored the ICME parameters obtained from OMNI-web<sup>7</sup> (NASA/GSFC). The average strength of the  $B$  field vector (G) was obtained to be  $9.4 \times 10^{-5}$  (G) (mean) with the mean flow speed of 369 km/s for the start and end date time of the ICME disturbance (see Figure 2). These values are consistent with those of the values in the Richardson–Cane catalogue.

#### 3.2. Statistical study of split-band type II bursts

Similarly, we derived the  $B$  field strength values ( $B_{\text{Radio}}$  (G)) for 31 such split-band observations for the solar cycles of 23 and 24, varying from 0.04 G to 4.59 G for the heliocentric distance ( $r$ ) ranging from  $1.1 R_{\odot}$  to  $2.5 R_{\odot}$ . We note that the 'a' in the Equation (2) varies for individual split-band observations. We calcu-

<sup>7</sup> <https://omniweb.gsfc.nasa.gov/index.html>

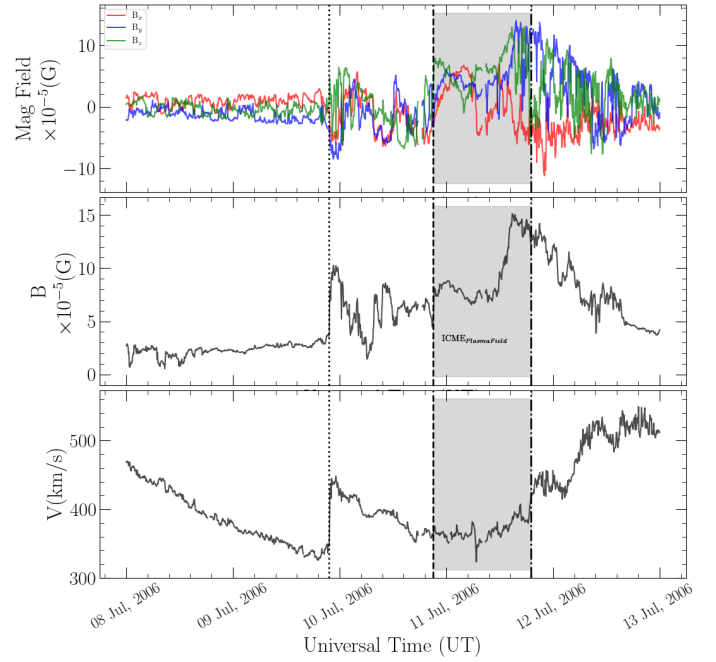


**Fig. 2.** Associated plot of ICME parameters obtained from OMNI data for the type II burst and CME that occurred on 6 July 2006. The top panel illustrates the  $B_x$ ,  $B_y$ , and  $B_z$  vector components of the  $B$  field (G); the middle panel shows the average strength of the  $B$  field vector (G); and the bottom panel shows the flow speed across the timeline of the event. The vertical dotted line shows the near-Earth shock arrival at 21:36 UT on 9 July 2006 and the grey-shaded region shows the start and end time of the disturbance in the plasma (Richardson & Cane 2010), starting at 19:00 UT on 9 July 2006 and ending at 21:00 UT on 11 July 2006.

lated the upstream magnetic field values,  $B_{1\text{AU}}$  (G) at 1 AU in the range  $4.5\text{--}20.8 \times 10^{-5}$  G obtained from the OMNI database. A correlation between the near-Sun coronal magnetic fields and near-Earth upstream magnetic field strength observed just before the ICME was established by linearly fitting the magnetic fields ( $B_{1\text{AU}}$  (G)) at 1 AU and the estimated ( $B_{\text{Radio}}$  (G)) was derived from the type II radio bursts (see Fig. 3), yielding a slope of 0.36 and an intercept of 8.19, suggesting a linearly weak relation. The weak correlation was confirmed by the obtained correlation coefficient ( $r$  of 0.14; see Fig. 3).

We used a four-fold Newkirk density model to estimate the shock heights (the radial distance from the Sun's centre to the leading edge of the shock wave that forms ahead of a CME as it propagates through the solar corona), in terms of  $R_{\odot}$ , close to the corona. We used three-fold and five-fold Newkirk density models to estimate the error bars for these shock height values (see Fig. 3). These height estimate errors were then used to set the upper and lower limits of the error bars in the shock speed calculations. Similarly, we averaged over  $\approx 15$  min of upstream magnetic field values at 1 AU and used the rms values to estimate the uncertainties in  $B_{1\text{AU}}$  (G) values in the pre-shock region (see Fig. 3). The uncertainties in the speed of CME ( $V_{\text{CME}}$ ) were estimated assuming linear propagation of the CME leading edge. The resulting uncertainties in the present study and correlation coefficients with error bars are shown in Fig. 3.

### 4. Summary and discussion

Figure 3 shows that the magnetic fields near the Sun estimated using radio techniques are not well correlated with the

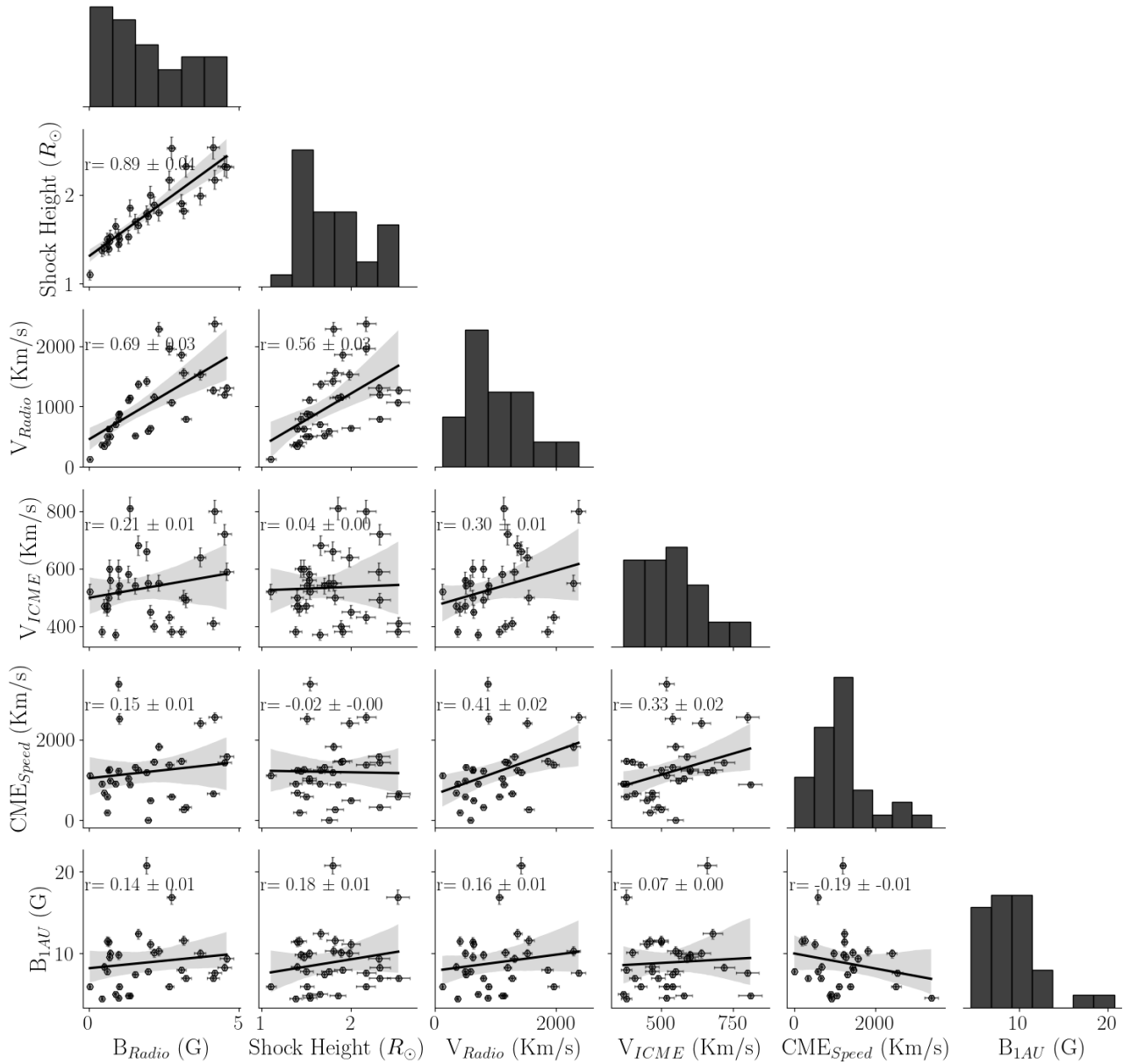


**Fig. 3.** Correlation between various parameters of 31 CME- and ICME-related events. The scattered hexagonal points are the data that contain shock height ( $R_{\odot}$ ),  $F_{\text{start}}$  (MHz),  $F_{\text{end}}$  (MHz), speed of radio bursts (km/s), ICME speed (km/s), CME speed (km/s), and magnetic field strength derived from type IIs and obtained with ICME in situ measurements.

magnetic field measured at 1 AU using in situ observations. Previous studies have suggested that metric radio observations can serve as effective proxies for estimating magnetic fields near the Sun (Vršnak & Cliver 2008; Kumari et al. 2017a, and the reference therein). However, to the best of our knowledge, there are no event specific or comprehensive long-term studies using solar radio bursts to estimate the heliospheric magnetic fields. Our findings in this study (see Fig. 3 and Table A.2) strongly indicate that no linear relation could be established using metric radio emissions to estimate the magnetic fields at 1 AU with acceptable error margins. This suggests that metric radio observations cannot serve as effective proxies for estimating magnetic fields close to the Earth. This could be due to the complex evolution of the magnetic field structures as it propagates through the heliosphere (see for a review, Owens & Forsyth 2013). It is well known that CMEs are subject to rotation, deflection, and interaction (with

solar wind and/or CME-CME interaction) (Palmerio et al. 2021; Sioulas et al. 2023, and the reference therein). However, we have not accounted for these conditions in our study due to the non-availability of radio data points between  $\approx 2 R_{\odot}$  and 1 AU, which are to be investigated in further studies with the availability of Parker Solar Probe (PSP) and Solar Orbiter (SoIo) data. The CME-ICME speed is correlated, suggesting that other factors such as speed can help understand the predictive patterns.

This study and the findings of this article can be summarized as follows:

1. Estimated  $B$  fields in the middle corona using split-band: We used the split-band observations to estimate magnetic fields within the middle corona. The split-band technique is an indirect measurement of magnetic field strengths just above the CME-driven shock, performed by analyzing different frequency bands of type II radio bursts.

2. Statistical analysis of radio bursts associated with ICMEs: Through statistical analysis, we investigated radio bursts associated with ICMEs. We also examined the start and end frequencies, bandwidths, and duration of radio emissions observed during ICME events. We aimed to identify a relation indicative of magnetic field variations and associated CMEs and ICMEs.
3. Relation between the magnetic field near the Sun and at 1 AU: Our results show almost no clear linear relation between the magnetic field strength near the Sun obtained with metric radio observations and in situ measurements of the magnetic field associated with upstream and/or shock transition fields just before the ICME. Hence, we could not establish any empirical relation that provides a means to estimate the magnetic field intensity when the disturbance reaches the Earth, based on measurements obtained closer to the Sun. This indicates that metric radio observations have become less reliable for estimating magnetic fields closer to Earth.

*Acknowledgements.* AK acknowledges the ANRF Prime Minister Early Career Research Grant (PM ECRG) program. The authors acknowledge the Param Vikram-1000 High Performance Computing Cluster of the Physical Research Laboratory (PRL). All the authors acknowledge the event lists provided by the Space Weather Prediction Center and the ICME catalogue compiled by Ian Richardson and Hilary Cane. The authors acknowledge the sunpy package, the Coordinated Data Analysis Workshop (CDAW) catalogue, Solar Electro-Optical Network's (SEON) Radio Spectral Telescope Network (RSTN) data, eCallisto data, National Institute of Information and Communications Technology's (NICT) Hiraio Radio Spectrograph (HiRAS) data, Solar and Heliospheric Observatory's (SOHO) Large Angle and Spectrometric Coronagraph (LASCO), and NASA/GSFC's OMNIweb database.

## References

- Brueckner, G. E., Howard, R. A., Koomen, M. J., et al. 1995, *Sol. Phys.*, **162**, 357
- Carley, E. P., Vilmer, N., Simões, P. J. A., & Ó Ferraigh, B. 2017, *A&A*, **608**, A137
- Carley, E. P., Vilmer, N., & Vourlidas, A. 2020, *Front. Astron. Space Sci.*, **7**, 79
- Cho, K.-S., Lee, J., Gary, D. E., Moon, Y.-J., & Park, Y. D. 2007, *ApJ*, **665**, 799
- Dulk, G. A., & McLean, D. J. 1978, *Sol. Phys.*, **57**, 279
- Dulk, G. A., & Suzuki, S. 1980, *A&A*, **88**, 203
- Gopalswamy, N. 2006, *Washington DC American Geophysical Union Geophysical Monograph Series*, **165**, 207
- Gopalswamy, N., & Yashiro, S. 2011, *ApJ*, **736**, L17
- Gopalswamy, N., Lara, A., Lepping, R. P., et al. 2000, *Geophys. Res. Lett.*, **27**, 145
- Jess, D. B., Reznikova, V. E., Ryans, R. S. I., et al. 2016, *Nat. Phys.*, **12**, 179
- Kahler, S. W., Ling, A. G., & Gopalswamy, N. 2019, *Sol. Phys.*, **294**, 134
- Kondo, T., Isobe, T., Igi, S., Watari, S., & Tokumaru, M. 1995, *J. Commun. Res. Lab.*, **42**, 111
- Kumari, A., Ramesh, R., Kathiravan, C., & Wang, T. J. 2017a, *Sol. Phys.*, **292**, 161
- Kumari, A., Ramesh, R., Kathiravan, C., & Wang, T. J. 2017b, *Sol. Phys.*, **292**, 177
- Kumari, A., Ramesh, R., Kathiravan, C., Wang, T. J., & Gopalswamy, N. 2019, *ApJ*, **881**, 24
- Kumari, A., Morosan, D. E., Kilpua, E. K. J., & Daei, F. 2023, *A&A*, **675**, A102
- Lin, H., Kuhn, J. R., & Coulter, R. 2004, *ApJ*, **613**, L177
- Mahrous, A., Alielden, K., Vršnak, B., & Youssef, M. 2018, *JASTP*, **172**, 75
- Newkirk, G., Jr. 1961, *ApJ*, **133**, 983
- Owens, M. J., & Forsyth, R. J. 2013, *Liv. Rev. Sol. Phys.*, **10**, 5
- Palmerio, E., Nieves-Chinchilla, T., Kilpua, E. K. J., et al. 2021, *J. Geophys. Res. Space Phys.*, **126**, e2021JA029770
- Ramesh, R., & Sastry, C. V. 2000, *A&A*, **358**, 749
- Richardson, I. G., & Cane, H. V. 2010, *Sol. Phys.*, **264**, 189
- Riley, P., Lionello, R., Mikić, Z., & Linker, J. 2008, *ApJ*, **672**, 1221
- Sioulas, N., Huang, Z., Shi, C., et al. 2023, *ApJ*, **943**, L8
- Smerd, S. F., & Sheridan, K. V. 1974, in *Coronal Disturbances*, ed. G. A. Newkirk, *Proc. IAU Symp.*, **57**, 389
- Smerd, S. F., Sheridan, K. V., & Stewart, R. T. 1975, *Astrophys. Lett.*, **16**, 23
- Vršnak, B., & Cliver, E. W. 2008, *Sol. Phys.*, **253**, 215
- Vršnak, B., Magdalenic, J., Aurass, H., & Mann, G. 2002, *A&A*, **396**, 673
- White, S. M. 2002, in *American Astronomical Society Meeting Abstracts*, **200**, 49.03
- White, S. M. 2004, *Astrophysics and Space Science Library*, **314**, 89
- Wiegmann, T., Petrie, G. J. D., & Riley, P. 2017, *Space Sci. Rev.*, **210**, 249
- Yashiro, S., Gopalswamy, N., Michalek, G., et al. 2004, *J. Geophys. Res. Space Phys.*, **109**, A07105

**Appendix A: Tables containing detailed information about the events studied.****Table A.1.** Various parameters of type II bursts and CMEs associated with the ICMEs in Table A.2

Date	Type II				CME					
	Time $T_{start}$ (UT)	$T_{end}$ (UT)	$T_{duration}$ (min)	Shock Height ( $R_{\odot}$ )	Frequency $F_{start}$ (MHz)	$F_{end}$ (MHz)	BW (MHz)	$T_{start}$ (UT)	Width (deg)	$v_{CME}$ (km/s)
12 Feb 2000	04:06	04:17	11	1.10	80	30	50	04:31	360	1107
16 Sep 2000	04:17	04:33	16	1.44	180	25	155	05:18	360	1215
25 Nov 2000	01:07	01:16	09	1.50	147	25	122	01:31	360	2519
10 Apr 2001	05:13	05:17	04	1.98	80	30	50	05:30	360	2411
09 Oct 2001	10:54	11:02	08	1.53	180	25	155	11:30	360	973
17 Nov 2001	04:50	04:55	05	2.16	145	45	100	05:30	360	1379
22 Nov 2001	22:31	22:41	10	2.32	116	25	91	23:30	360	1437
26 Dec 2001	05:02	05:19	17	1.88	180	25	155	05:30	212	1446
17 Apr 2002	08:08	08:23	15	1.39	79	25	54	08:26	360	1240
29 Jul 2002	02:40	02:43	03	1.42	270	65	205	12:07	095	190
29 May 2003	01:06	01:11	05	1.66	80	30	50	01:27	360	1237
12 Sep 2004	01:41	01:50	09	1.76	180	57	123	00:36	360	1328
10 Nov 2004	02:07	02:15	08	1.54	260	70	190	02:26	360	3387
17 Jan 2005	09:44	09:47	03	2.17	65	25	40	09:30	360	2547
20 Jan 2005	06:44	07:00	16	1.85	180	160	20	06:54	360	882
22 Aug 2005	01:02	01:08	06	1.79	60	30	30	01:31	360	1194
06 Jul 2006	08:24	08:41	17	1.38	180	25	155	08:54	360	911
14 Dec 2006	22:09	22:13	04	1.53	180	25	155	22:30	360	1042
15 Feb 2011	01:52	02:00	08	1.40	260	57	203	02:36	360	669
04 Aug 2011	03:54	04:03	09	1.70	180	66	114	04:12	360	1315
06 Sep 2011	22:19	22:34	15	1.50	300	40	260	23:05	360	575
09 Nov 2011	13:11	13:31	20	1.65	180	30	150	13:30	360	907
19 Jan 2012	12:52	13:01	09	2.00	084	29	055	14:36	065	498
07 Mar 2012	01:09	01:29	20	1.80	180	25	155	00:24	360	1825
04 Jul 2012	16:42	17:04	22	2.53	181	25	156	17:24	360	662
12 Jul 2012	16:25	16:53	28	2.32	82	25	57	16:48	025	329
02 Apr 2014	13:23	13:25	02	1.91	121	28	93	13:48	360	1471
10 Sep 2014	17:27	17:57	30	1.48	180	25	155	18:00	360	1267
17 Dec 2014	04:44	05:01	27	2.52	70	23	47	05:00	360	587
04 Nov 2015	03:23	03:34	11	1.82	180	41	139	14:48	064	272
06 Sep 2017	12:02	12:21	19	2.31	081	25	56	12:24	360	1571

**Table A.2.** Various ICME parameters associated with the type II bursts and CMEs in Table A.1

ICME										
Date	Disturbance		ICME Plasma/Field							
	Time $T_s$ (UT)	Start Date	$T_{start}$ (UT)	End Date	$T_{end}$ (UT)	ICME <sub>plasma</sub> Speed (km/s)	$V_{max}$ (km/s)	$B_{1AU}$ ( $\times 10^{-5}(G)$ )	$V_{Radio}$ (km/s)	$B_{Radio}$ (G)
14 Feb 2000	07:31	14 Feb 2000	12:00	16 Feb 2000	08:00	520	680	6	122	0.04
17 Sep 2000	16:57	17 Sep 2000	21:00	21 Sep 2000	00:00	600	840	9.8	793	0.99
28 Nov 2001	05:30	28 Nov 2001	11:00	29 Nov 2001	22:00	540	580	6	883	1.01
11 Apr 2001	13:43	11 Apr 2001	22:00	13 Apr 2001	07:00	640	740	10	1525	3.71
11 Oct 2001	17:01	12 Oct 2001	04:00	12 Oct 2001	09:00	560	570	10	503	0.71
19 Nov 2001	18:15	19 Nov 2001	22:00	21 Nov 2001	13:00	430	570	6	1953	2.69
24 Nov 2001	06:56	24 Nov 2001	14:00	25 Nov 2001	20:00	720	1040	8.3	1196	4.52
29 Dec 2001	05:38	30 Dec 2001	00:00	30 Dec 2001	18:00	400	460	10.1	1158	2.17
19 Apr 2002	08:35	20 Apr 2002	00:00	21 Apr 2002	18:00	500	640	11.4	0624	0.65
01 Aug 2002	23:09	02 Aug 2002	06:00	04 Aug 2002	02:00	460	520	11.5	404	0.60
30 May 2003	16:00	30 May 2003	22:00	01 Jun 2003	01:00	680	780	12.4	1364	1.66
13 Sep 2004	20:03	14 Sep 2004	15:00	16 Sep 2004	12:00	550	600	7.8	586	1.97
11 Nov 2004	17:10	12 Nov 2004	08:00	13 Nov 2004	23:00	520	670	4.6	869	0.99
18 Jan 2005	21:00	18 Jan 2005	23:00	20 Jan 2005	03:00	800	960	7.6	2369	4.20
21 Jan 2005	17:11	21 Jan 2005	19:00	22 Jan 2005	17:00	810	960	4.8	1138	1.38
24 Aug 2005	06:13	24 Aug 2005	14:00	24 Aug 2005	23:00	660	710	20.8	1417	1.93
09 Jul 2006	21:36	10 Jul 2006	21:00	11 Jul 2006	19:00	380	430	4.5	369	0.45
16 Dec 2006	17:55	17 Dec 2006	00:00	17 Dec 2006	17:00	580	680	4.8	1106	1.31
18 Feb 2011	01:30	18 Feb 2011	19:00	20 Feb 2011	08:00	470	600	8.4	346	0.52
05 Aug 2011	17:51	06 Aug 2011	22:00	07 Aug 2011	22:00	540	610	7.4	513	1.54
09 Sep 2011	12:42	10 Sep 2011	03:00	10 Sep 2011	15:00	470	530	7.8	501	0.61
12 Nov 2011	05:59	13 Nov 2011	10:00	15 Nov 2011	02:00	370	460	5	703	0.88
22 Jan 2012	06:11	22 Jan 2012	23:00	23 Jan 2012	07:00	450	460	11.1	640	2.05
08 Mar 2012	11:03	09 Mar 2012	03:00	11 Mar 2012	07:00	550	890	10.3	2285	2.33
08 Jul 2012	08:00	09 Jul 2012	00:00	09 Jul 2012	14:00	410	450	7	1269	4.14
14 Jul 2012	18:09	15 Jul 2012	06:00	17 Jul 2012	05:00	490	670	7	794	3.25
05 Apr 2014	10:00	05 Apr 2014	22:00	07 Apr 2014	05:00	380	500	8	1853	3.09
12 Sep 2014	15:53	12 Sep 2014	22:00	14 Sep 2014	02:00	600	720	9.6	626	0.68
21 Dec 2014	19:11	22 Dec 2014	04:00	22 Dec 2014	17:00	380	430	17	1063	2.74
06 Nov 2015	1818	07 Nov 2015	06:00	08 Nov 2015	16:00	500	680	11.6	1550	3.16
07 Sep 2017	2302	08 Sep 2017	11:00	10 Sep 2017	21:00	590	800	9.4	1303	4.59